Applied Physics Letters

Demonstration of microwave plasmonic-like vortices with tunable topological charges by a single metaparticle

Cite as: Appl. Phys. Lett. **118**, 241106 (2021); https://doi.org/10.1063/5.0053834
Submitted: 12 April 2021 . Accepted: 01 June 2021 . Published Online: 16 June 2021

Guangxu Su, Hai Su, Lumang Hu, Zhaofu Qin, Xiaopeng Shen, Jianping Ding, Fanxin Liu, Minghui Lu, Peng Zhan, and Yongmin Liu

Applied Physics Letters ARTICLE scitation.org/journal/apl

Demonstration of microwave plasmonic-like vortices with tunable topological charges by a single metaparticle

Cite as: Appl. Phys. Lett. **118**, 241106 (2021); doi: 10.1063/5.0053834
Submitted: 12 April 2021 · Accepted: 1 June 2021 ·
Published Online: 16 June 2021

Guangxu Su,[1,2] Hai Su,[1] Lumang Hu,[1] Zhaofu Qin,[1] Xiaopeng Shen,[3] Jianping Ding,[1] Fanxin Liu,[2] Minghui Lu,[4] Peng Zhan,[1,a)] and Yongmin Liu[5,a)]

AFFILIATIONS

[1]National Laboratory of Solid State Microstructures and Collaborative Innovation Center of Advanced Microstructures, School of Physics, Nanjing University, Nanjing 210093, China
[2]Department of Applied Physics, Zhejiang University of Technology, Hangzhou 310023, China
[3]School of Physical Science and Technology, China University of Mining and Technology, Xuzhou 221116, China
[4]National Laboratory of Solid State Microstructures and Collaborative Innovation Center of Advanced Microstructures, Department of Materials Science and Engineering, Nanjing University, and Jiangsu Key Laboratory of Artificial Functional Materials, Nanjing 210093, China
[5]Department of Mechanical and Industrial Engineering and Department of Electrical and Computer Engineering, Northeastern University, Boston, Massachusetts 02115, USA

[a)]**Authors to whom correspondence should be addressed:** zhanpeng@nju.edu.cn and y.liu@northeastern.edu

ABSTRACT

Light beams with helical wave fronts, also called optical vortices, have attracted great interest in the community of optics and photonics. They provide an additional degree of freedom for light manipulation, leading to wide-ranging potential applications in micro-particle trapping, optical microscopy, and even quantum information processing. Recently, metallic microstructures are introduced to confine the plasmonic vortices into deep subwavelength dimension, which benefits photonic integration on chip. In this Letter, exploiting the excitation of spoof surface plasmon, we experimentally demonstrate the near-field optical vortices with tunable topological charges supported by a single metaparticle in the microwave regime. These microwave plasmonic-like vortices are excited by surface waves with a spatial asymmetric distribution of electromagnetic field, which are launched by a metallic comb-shaped waveguide. Experimental characterization of highly localized and controllable near-field vortices with the nature of deep subwavelength confirms the numerical simulation. In addition, an equivalent physical model based on the coupled mode theory is proposed to understand the generation mechanism of these spoof plasmonic vortices. Our approach offers an efficient way to generate deterministic subwavelength optical vortices, which provides the potential for critical vortex elements on photonic integrated chip.

The angular momentum of light is one of the most fundamental physical quantities in optics and photonics, which comprises two intrinsic components, namely spin angular momentum (SAM) and orbital angular momentum (OAM). It is well known that circularly polarized light carries SAM given by $\pm\hbar$ per photon. In contrast, OAM is associated with electromagnetic (EM) waves possessing helical phase front distributions,[1–3] which has the value of $l\hbar$ per photon with the topological charge l being an arbitrary integer. To date, OAM beams, commonly referred to as optical vortices, have given rise to many developments in the fields of optical communication,[4] data storage,[5] optical micromanipulation,[6] astronomy,[7] etc. Optical vortices with free-space form have been efficiently generated by spiral phase plates,[8] spatial light modulators,[9] and computer-generated holograms.[10]

Recently, in pursuit of further miniaturization of optical vortex generator for growing demands of photonic integration, some approaches by using metasurfaces[11,12] and compact ring resonators[13,14] have been developed. In particular, plasmonic vortices have attracted extensive attention.[15–20] Compared with free-space optical vortices, one of the greatest advantages of plasmonic vortices lies in

the fact that they can confine optical fields carrying OAM to subwavelength scales beyond the diffraction limit, which means that it may enable potential applications in nano-manipulation,[15] super resolution imaging,[16] and subwavelength optical elements for optical information processing.[17] Thus far, various elaborate plasmonic geometries, such as Archimedes spiral, chiral slits, and rings on a flat metal surface, have been proposed to generate near-field subwavelength vortices carrying specific topological charges through an excitation of surface plasmon polaritons (SPPs) under different polarized illuminations.[21–23] However, plasmonic vortices are inherently limited to visible and near-infrared frequencies, because at low frequencies, metals like gold and copper are akin to perfect electric conductors (PEC), which cannot induce surface plasmons (SPs) wave at metal/dielectric interface. To tackle this issue, the concept of spoof SPs has been brought forward to convert free-space EM waves at low frequency into surface waves.[24–30] It is found that structured metals with subwavelength grooves or holes can support confined low-frequency EM modes, regarded as analogue of SPP in the visible and near-infrared region. On this basis, plasmonic-like vortices with specific topological charge have recently been presented in the microwave regime by utilizing well-designed subwavelength microstructures.[31–33] It is highly desirable to generate flexibly low-frequency plasmonic vortex carrying OAM, which may provide abundant applications in integrated microcircuits for information encoding, data storage, and complex logical operation.

In this Letter, we demonstrate a subwavelength metaparticle for the generation of microwave near-field vortices carrying well-defined OAM. These variable plasmonic-like vortices can be selectively excited by a spatial asymmetric field that is produced by the evanescent wave of a spoof SPP from an access comb-shaped waveguide. We experimentally and numerically demonstrate the electromagnetic field properties of these strongly localized plasmonic vortices by mapping the field intensity and phase distribution through the microwave near-field scanning setup. In addition, we study systematically the electromagnetic field transmission characteristics of well-designed metaparticle-waveguide system and propose an equivalent physical model based on the coupled mode theory (CMT) to reveal the mechanism of plasmonic-like vortices generations. Due to its characteristics of strong-field confinement, deep subwavelength, and mode flexibility, the metaparticle that we proposed would provide abundant applications in integrated microcircuits for information encoding, data storage, and complex logical operation. On the other hand, in principle, our design can be scaled to high frequency (such as terahertz and infrared) regime by using microfabrication and that would provide a way to study the light–matter interaction with localized plasmonic vortex, supporting some specific applications, such as chiral quantum emitters and optical trapping.

The metaparticle that we designed is a 3D rim-textured metallic disk corrugated with circularly periodic grooves as shown schematically in the inset of Fig. 1(a). Here, as a specific example, the equivalent radius (R) and thickness (t) of this textured metallic particle are set as 8 mm and 0.018 mm, respectively. The inner radius (r) and the duty cycle (b/a) of this textured metallic particle are set as 2 mm and 0.4, respectively. This metaparticle is placed on a 0.5 mm-thick (d) dielectric layer with a relative permittivity of 2.55. The number of grooves (N) is chosen as 48. To study the EM properties of such a metaparticle, we numerically characterize the near-field EM response by locating an

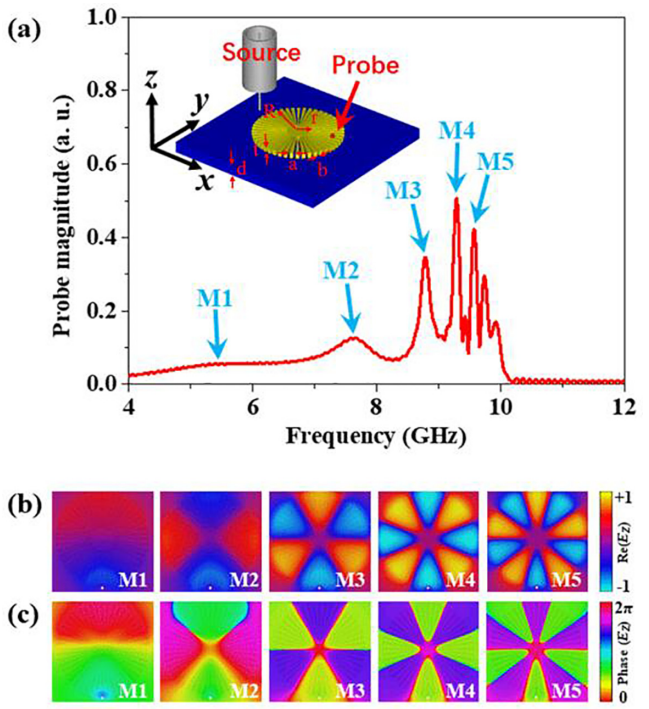

FIG. 1. Multiple spoof LSP resonances supported by a textured metallic metaparticle. (a) Near-field response spectrum of the metaparticle, in which five typical resonant peaks ($M1$–$M5$, with frequency of 5.37, 7.82, 8.83, 9.30, and 9.57 GHz) are marked with blue arrows. Near-field intensity (b) and phase (c) distributions of E_Z component for the five marked resonances. The plots are in the x–y plane 1 mm above the metaparticle.

excitation source and a field monitor at proper positions. The simulated near-field response spectrum, reflecting the extinction property of this metaparticle, is described as the energy magnitude of the detected field as a function of the frequency, which is calculated by the commercial software CST Microwave Studio. In Fig. 1(a), a set of separated peaks can be clearly observed. By mapping the electric field patterns corresponding to the selected five modes (marked as $M1 - M5$), we can confirm that these modes are directly related to the excited spoof localized surface plasmon (LSP) resonances of such a metallic metaparticle, as presented in Fig. 1(b). The corresponding phase distributions of these five resonances exhibit discrete phase discontinuities (about $\pi/2$ or $3\pi/2$) along the azimuthal direction of the metaparticle as shown in Fig. 1(c), which means these spoof LSP resonances do not carry OAM.

Extensive research demonstrates that the evanescent fields of a waveguide not only provide tightly confined EM field for an enhanced light–matter interaction, but also can offer an opportunity to manipulate the resonant and scattering behaviors of the surrounding microparticle.[34,35] In our scheme, a spoof SPP waveguide with a comb-shaped ideal-metal stripe is designed on a 0.5 mm-thick dielectric slab with a relative permittivity of 2.55, of which the periodicity (p) and metal stripe-width (c) are set as 5 mm and 2 mm, respectively. (The other geometry parameters of this waveguide are provided in the supplementary material.) In fact, the equivalent dispersion of spoof

SPP mode strongly depends on the depth (h) of grooves, as shown in Fig. S1. According to our simulation, h is optimized to be 4 mm to ensure that spoof SPP can be more tightly confined to this comb-shaped structure. Note that, in order to achieve high-efficiency conversion from traditional guided waves to spoof SPP, we apply a conversion structure consisting of gradient corrugated grooves and flaring grounds. Within the frequency band from 4 to 12 GHz of our interest, this well-designed hybrid waveguide, consisting of coplanar waveguides, conversion structures, and spoof SPP waveguide, exhibits high transmission coefficient (red line, S_{21}) and low reflection coefficient (black line, S_{11}), as shown in Figs. S2 and S3. Here, we define the left (right) side of the hybrid waveguide as Port 1(2). In addition to the propagating nature of spoof SPP wave along the micro-structured surface, the field perpendicular to the surface decaying exponentially away from the surface gives rise to the asymmetric spatial distribution of evanescent field, which might strongly influence on the near-field characteristics of adjacent target metallic micro-particle.

As illustrated in the inset of Fig. 2(a), we put the textured metallic metaparticle close to the spoof SPP waveguide with an edge-distance of $g = 4$ mm. The red arrow indicates the propagation direction of launched spoof SPP wave. The waveguide–metaparticle interaction due to the evanescent coupling could be reflected by the intensity and phase information of transmission (S_{21}) spectrum from the output port of the hybrid waveguide that we construct. Thus, shown as the red curve in Fig. 2(a), through computing the transmission/reflection (S_{21}/S_{11}) spectra of the spoof SPP along the surface waveguide with a single metaparticle in the vicinity of it, we can clearly find a series of spectral dips in the transmission spectrum, marked as mode $m1 - m5$. The near-field patterns of E_z component of these modes in the x–y plane, which are plotted at the plane of 1 mm above the metaparticle, indicate that these localized resonances supported by metaparticle are evanescently coupled from the comb-shaped waveguide. By comparing with Fig. 1, we could find that that these localized modes of metaparticle excited by evanescent field of spoof SPP waveguide almost coincide in frequency with the spoof LSP resonances and show the same transient electric field distributions as shown in Fig. 2(b). In order to further study the nature of these resonant modes, the corresponding normalized instantaneous phase distribution of E_z component is plotted. Phase gradients along the azimuthal direction are presented, which is in a sharp contrast to Fig. 1(c). In Fig. 2(c), the phase increases continuously counterclockwise around the center by 2π, 4π, 6π, 8π, and 10π, corresponding to the modes marked from $m1$ to $m5$, respectively. The results manifest that these generated near-field modes ($m1 - m5$) carry OAM with topological charge from -1 to -5. Interestingly, due to the symmetry of this waveguide-metaparticle system, evanescent field in the reverse propagation direction along the spoof SPP waveguide can excite the localized modes of a single metaparticle carrying OAM with topological charge from 1 to 5. (Results are shown in Fig. S4.)

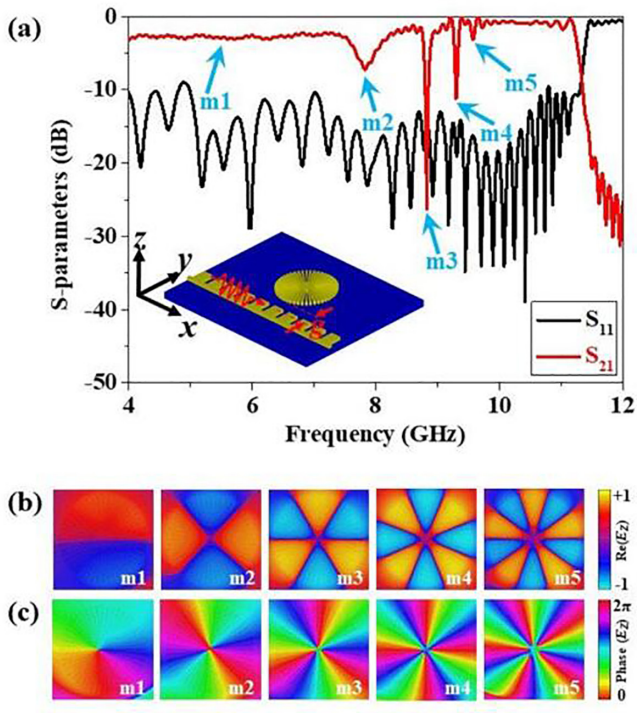

FIG. 2. Numerical simulations of spoof LSP vortices supported by the metaparticle. (a) Transmission (red curve, S_{21}) and reflection (black-curve, S_{11}) coefficients of the metaparticle-waveguide system by detecting the electric fields of the waveguide ports. Spectral dips ($m1$–$m5$) marked by the blue arrows indicate multiple spoof LSP modes carrying OAM with topological charge from -1 to -5, respectively. Corresponding near-field intensity (b) and phase (c) distributions of E_Z component for multiple spoof LSP vortices in the x–y plane 1 mm above the metaparticle.

To demonstrate these plasmonic-like vortices experimentally, a sample is fabricated on a ∼0.5 mm-thick F4B plate with relative permittivity of ∼2.55 by using a conventional printed-circuit-board process. The geometries of the prepared sample, including the metaparticle and the comb-shaped metallic waveguide, are the same as those of the numerical models as mentioned before, and the photographs of fabricated sample are provided in Fig. S5. As shown in the inset of Fig. 3(a), the propagation direction of the launched spoof SPP wave is indicated by the red wavy-line with arrow. The spectral EM responses and the corresponding field properties (including field intensity and phase distributions of E_z component) are measured by a vector network analyzer (Agilent E5063A). The energy coupling process from the access spoof SPP waveguide to the metallic metaparticle can be illustrated by the measurement of transmittance (S_{21}) at the right port of the comb-shaped waveguide. As shown by the measured transmission (S_{21}) and reflection (S_{11}) coefficients in Fig. 3(a), we can identify five spectral transmission dips marked as $m1 - m5$. The measured transmission (or reflection) spectrum fits the numerically simulated one very well except for some slight differences of the modes' frequencies between them, which might be attributed to the geometry deviation between fabricated sample and the numerical design. Note that the oscillation of S-parameters comes from the slight impedance mismatch between microwave connectors and the designed hybrid waveguide. In order to experimentally verify the excited localized modes held by metaparticle, which is predicted numerically to carry OAM, a dipole antenna as a detector is fixed at ∼1 mm above the metaparticle and moved in x–y plane to scan the field magnitude of E_z and its phase as well. These data are recorded by vector network analyzer to depict the field pattern. Figures 3(b) and 3(c) present the measured amplitude intensity and phase distributions of the near-field distributions of spoof LSP modes. Apparently, these modes localized

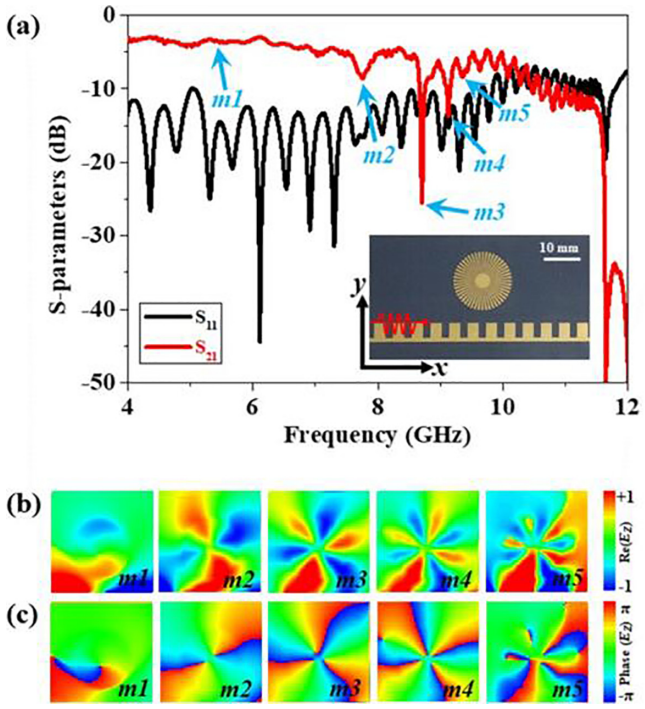

FIG. 3. Measured results of spoof LSP vortices. (a) Measured transmission (red curve, S_{21}) and reflection (black-curve, S_{11}) spectra of the metaparticle-waveguide system. Measured spectral dips ($m1$–$m5$) marked by blue arrows indicate plasmonic-like vortices with topological charge from −1 to −5, respectively. Near-field intensity (b) and phase (c) distributions of E_Z component for vortex modes corresponding to (a) in the x–y plane 1 mm above the metaparticle.

by metaparticle possess characteristics of vortex with topological charges $-1\sim-5$ from low to high frequency, which is in good agreement with the simulation results.

Furthermore, we employ a simplified equivalent model based on the coupled mode theory (CMT) to investigate the generation mechanism of spoof LSP vortices by analyzing the EM field transmission behavior of this waveguide-metaparticle system. First, by comparing Figs. S2(e) and 2(a), we can see that the overall transmission of spoof SPP could be evidently modulated by the adjacent metaparticle. However, this metaparticle has indeed negligible impact on the reflection efficiency of hybrid waveguides. Therefore, as schematically illustrated in Fig. 4(a), the reflection of spoof SPP wave is not considered in this model, which means only the transmission and the trapped energy by metaparticle are taken into account. In this case, similar to the discussion of coupling process about fiber ring resonators,[36,37] the following matrix can be used to describe the coupled system:

$$\begin{bmatrix} E_2 \\ E_3 \end{bmatrix} = \begin{bmatrix} \alpha & i\beta \\ i\beta & \alpha \end{bmatrix} \begin{bmatrix} E_1 \\ E_4 \end{bmatrix}, \tag{1}$$

which illustrates the mode coupling between the comb-shaped waveguide and the metaparticle, with α and β representing the coupling parameters. For simplicity, we assume that the coupling between this waveguide-metaparticle system is lossless, so the coupling parameters α and β satisfy $\alpha^2+\beta^2=1$. On the other hand, considering the inevitable radiative loss and bending loss, the spoof LSP vortex supported by the metaparticle could be described by

$$E_4 = (1-\gamma)\exp(j\theta)\,E_3. \tag{2}$$

Here γ is the attenuation factor of the near-field amplitude due to the losses and θ stands for the phase distribution along the azimuthal direction of our proposed metaparticle. Combining Eqs. (1) and (2), we can obtain the normalized transmission coefficient ($|E_2|/|E_1|$) of the waveguide-metaparticle given as the following expression:

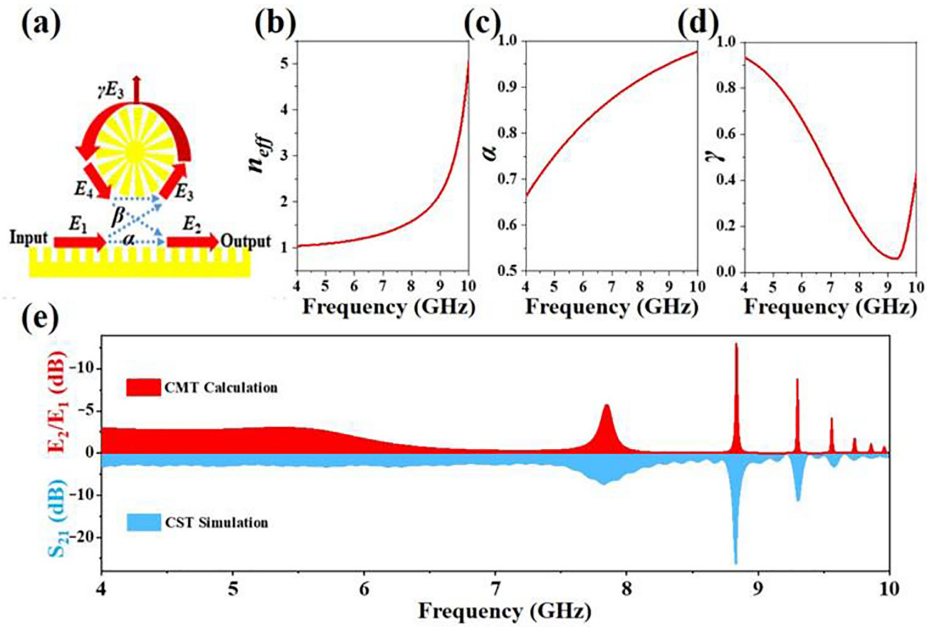

FIG. 4. Modal properties of spoof plasmons and their coupling mechanism based on the coupled mode theory (CMT). (a) Equivalent model revealing the mechanism of spoof LSP carrying OAM. (b)–(d) Effective index n_{eff} of the metaparticle, coupling parameters α of the coupled system, and attenuation factor γ of the near-field amplitude as the function of frequency, respectively. (e) CMT calculation (red) and CST simulation (blue) for the normalized transmission coefficient.

$$\frac{|E_2|}{|E_1|} = \sqrt{\frac{(1-\gamma)^2 + \alpha^2 - 2(1-\gamma)\alpha\cos\theta}{1 + (1-\gamma)^2\alpha^2 - 2(1-\gamma)\alpha\cos\theta}}. \quad (3)$$

Noted that in Eq. (3), θ should be related to the effective index (n_{eff}) of metaparticle and the frequency (f) of the corresponding spoof LSP resonance, which can be described by

$$\theta = 2\pi \cdot \frac{2\pi R}{\lambda_{LSP}} = \frac{4\pi^2 R}{c} \cdot f \cdot n_{eff}. \quad (4)$$

n_{eff} is actually dependent on the frequency, as depicted in Fig. 4(b), which increases evidently with the increase of frequency f. Parameter α depends on the coupling strength between the waveguide and the metaparticle. When the frequency increases, EM field can be confined more tightly near the waveguide. Thus, α increases monotonously with the increase in frequency f, as shown in Fig. 4(c). It should be noted that there is no monotonic relationship between parameters γ and frequency f, as shown in Fig. 4(d). The inflection point of minimum loss appears near 9.3 GHz. When the frequency decreases from 9.3 GHz, the wavelength of these vortex modes becomes much larger than the whole structure of the metaparticle, and thus, the bending loss of these vortex modes becomes increasingly evident. When the frequency increases from 9.3 GHz, the wavelength of these vortex modes is comparable to the detailed structures of the metaparticle, and thus, the scattering loss of these vortex modes increases with the increase in frequency f. Considering these factors mentioned above, the predicated normalized transmission coefficient is given in Fig. 4(e), which fits well with the normalized transmission coefficient calculated by CST simulation.

In summary, we demonstrate an effective way to generate microwave plasmonic-like vortices carrying tunable order topological charges by a single metaparticle. These subwavelength near-field vortices from the rationally designed metaparticle could be selectively excited by the spatial asymmetric field of a spoof SPP wave launched by a comb-shape waveguide. To illustrate the generation of these plasmonic-like vortices, we propose an equivalent model based on the coupled mode theory by considering the equivalent dispersion, coupling strength, and radiation loss in our spoof plasmon scheme; the results of which fit those of experiments and numerical simulations very well. Our work provides an effective way for creating localized plasmon modes carrying OAM with flexibility and would enable promising applications in functional micro-components and photonic integrated devices.

See the supplementary material for the simulated dispersion relationship of spoof SPP, the schematic diagram and photographs of hybrid waveguide, the simulated and measured transmission (reflection) coefficient, the photographs and numerical simulation of metaparticle-waveguide systems.

AUTHORS' CONTRIBUTIONS

G.X.S. and H.S. contributed equally to this work.

This work was financially supported by National Key R&D Program of China (Nos. 2018YFA0306200 and 2017YFA0303702) and National Natural Science Foundation of China (Nos. 11674166, 11834007, 91750202, 11974015, and 11574270).

DATA AVAILABILITY

The data that support the findings of this study are available from the corresponding authors upon reasonable request.

REFERENCES

[1]L. Allen, M. W. Beijersbergen, R. J. C. Spreeuw, and J. P. Woerdman, "Orbital angular momentum of light and the transformation of Laguerre-Gaussian laser modes," Phys. Rev. A **45**, 8185 (1992).
[2]M. Padgett and R. Bowman, "Tweezers with a twist," Nat. Photonics **5**, 343 (2011).
[3]A. E. Willner, H. Huang, Y. Yan, Y. Ren, N. Ahmed, G. Xie, C. Bao, L. Li, Y. Cao, Z. Zhao, J. Wang, M. P. J. Lavery, M. Tur, S. Ramachandran, A. F. Molisch, N. Ashrafi, and S. Ashrafi, "Optical communications using orbital angular momentum beams," Adv. Opt. Photonics **7**, 66 (2015).
[4]J. Wang, J. Yang, I. M. Fazal, N. Ahmed, Y. Yan, H. Huang, Y. Ren, Y. Yue, S. Dolinar, M. Tur, and A. E. Willner, "Terabit free-space data transmission employing orbital angular momentum multiplexing," Nat. Photonics **6**, 488 (2012).
[5]A. Nicolas, L. Veissier, L. Giner, E Giacobino, D. Maxein, and J. Laurat, "A quantum memory for orbital angular momentum photonic qubits," Nat. Photonics **8**, 234 (2014).
[6]D. Baresch, J. L. Thomas, and R. Marchiano, "Orbital angular momentum transfer to stably trapped elastic particles in acoustical vortex beams," Phys. Rev. Lett. **121**, 074301 (2018).
[7]F. Tamburini, B. Thidé, G. Molina-Terriza, and G. Anzolin, "Twisting of light around rotating black holes," Nat. Phys. **7**, 195 (2011).
[8]A. M. Yao and M. J. Padgett, "Orbital angular momentum: Origins, behavior and applications," Adv. Opt. Photonics **3**, 161 (2011).
[9]G. Gibson, J. Courtial, M. J. Padgett, M. Vasnetsov, V. Pasko, S. M. Barnett, and S. Franke-Arnold, "Free-space information transfer using light beams carrying orbital angular momentum," Opt. Express **12**, 5448 (2004).
[10]G. C. Berkhout, M. P. Lavery, J. Courtial, M. W. Beijersbergen, and M. J. Padgett, "Efficient sorting of orbital angular momentum states of light," Phys. Rev. Lett. **105**, 153601 (2010).
[11]P. G. Nanfang Yu, M. A. Kats, F. Aieta, J. P. Tetienne, F. Capasso, and Z. Gaburro, "Light propagation with phase discontinuities generalized laws of reflection and refraction," Science **334**, 333 (2011).
[12]E. Karimi, S. A. Schulz, I. De Leon, H. Qassim, J. Upham, and R. W. Boyd, "Generating optical orbital angular momentum at visible wavelengths using a plasmonic metasurface," Light: Sci. Appl. **3**, e167 (2014).
[13]J. W. X. Cai, M. J. Strain, B. J. Morris, J. Zhu, M. Sorel, J. L. O'Brien, M. G. Thompson, and S. Yu, "Integrated compact optical vortex beam emitters," Science **338**, 363 (2012).
[14]J. Zhang, C. Sun, B. Xiong, J. Wang, Z. Hao, L. Wang, Y. Han, H. Li, Y. Luo, Y. Xiao, C. Yu, T. Tanemura, Y. Nakano, S. Li, X. Cai, and S. Yu, "An InP-based vortex beam emitter with monolithically integrated laser," Nat. Commun. **9**, 2652 (2018).
[15]W. Y. Tsai, J. S. Huang, and C. B. Huang, "Selective trapping or rotation of isotropic dielectric microparticles by optical near field in a plasmonic archimedes spiral," Nano Lett. **14**, 547 (2014).
[16]C. Zhang, C. Min, L. Du, and X. C. Yuan, "Perfect optical vortex enhanced surface plasmon excitation for plasmonic structured illumination microscopy imaging," Appl. Phys. Lett. **108**, 201601 (2016).
[17]D. Pan, H. Wei, L. Gao, and H. Xu, "Strong spin-orbit interaction of light in plasmonic nanostructures and nanocircuits," Phys. Rev. Lett. **117**, 166803 (2016).
[18]W. Y. Tsai, Q. Sun, G. W. Hu, P. C. Wu, R. J. Lin, C. W. Qiu, K. Ueno, H. Misawa, and D. P. Tsai, "Twisted surface plasmons with spin-controlled gold surfaces," Adv. Opt. Mater. **7**, 1801060 (2019).
[19]X. M. Hong, G. W. Hu, W. C. Zhao, K. Wang, S. Sun, R. Zhu, J. Wu, W. W. Liu, K. P. Loh, A. T. S. Wee, B. Wang, A. Alu, C. W. Qiu, and P. X. Lu, "Structuring nonlinear wavefront emitted from monolayer transition-metal dichalcogenides," Research **2020**, 1.
[20]Y. J. Yang, L. X. Wu, Y. D. Liu, D. K. Xie, Z. W. Jin, J. F. Li, G. W. Hu, and C. W. Qiu, "Deuterogenic plasmonic vortices," Nano Lett. **20**, 6774 (2020).

[21]Y. Gorodetski, A. Niv, V. Kleiner, and E. Hasman, "Observation of the spin-based plasmonic effect in nanoscale structures," Phys. Rev. Lett. **101**, 043903 (2008).
[22]D. K. G. Spektor, A. K. Mahro, B. Frank, S. Ristok, L. Gal, P. Kahl, D. Podbiel, S. Mathias, H. Giessen, F. J. Meyer zu Heringdorf, M. Orenstein, and M. Aeschlimann, "Revealing the subfemtosecond dynamics of orbital angular momentum in nanoplasmonic vortices," Science **355**, 1187 (2017).
[23]H. Kim, J. Park, S. W. Cho, S. Y. Lee, M. Kang, and B. Lee, "Synthesis and dynamic switching of surface plasmon vortices with plasmonic vortex lens," Nano Lett. **10**, 529 (2010).
[24]J. B. Pendry, L. Martín-Moreno, and F. J. Garcia-Vidal, "Mimicking surface plasmons with structured surfaces," Science **305**, 847 (2004).
[25]S. A. Maier, S. R. Andrews, L. Martín-Moreno, and F. J. García-Vidal, "Terahertz surface plasmon-polariton propagation and focusing on periodically corrugated metal wires," Phys. Rev. Lett. **97**, 176805 (2006).
[26]A. Pors, E. Moreno, L. Martin-Moreno, J. B. Pendry, and F. J. Garcia-Vidal, "Localized spoof plasmons arise while texturing closed surfaces," Phys. Rev. Lett. **108**, 223905 (2012).
[27]X. Shen, T. J. Cui, D. Martin-Cano, and F. J. Garcia-Vidal, "Conformal surface plasmons propagating on ultrathin and flexible films," Proc Natl. Acad. Sci. **110**, 40 (2013).
[28]H. F. .Ma, X. Shen, Q. Cheng, W. X. Jiang, and T. J. Cui, "Broadband and high-efficiency conversion from guided waves to spoof surface plasmon polaritons," Laser Photonics Rev. **8**, 146 (2014).
[29]P. A. Huidobro, X. Shen, J. Cuerda, E. Moreno, L. Martin-Moreno, F. J. Garcia-Vidal, T. J. Cui, and J. B. Pendry, "Magnetic localized surface plasmons," Phys. Rev. X **4**, 021003 (2014).
[30]X. Shen and T. J. Cui, "Ultrathin plasmonic metamaterial for spoof localized surface plasmons," Laser Photonics Rev. **8**, 137 (2014).
[31]H. Su, X. Shen, G. Su, L. Li, J. Ding, F. Liu, P. Zhan, Y. Liu, and Z. Wang, "Efficient generation of microwave plasmonic vortices via a single deep-subwavelength meta-particle," Laser Photonics Rev. **12**, 1800010 (2018).
[32]Z. Liao, J. N. Zhou, G. Q. Luo, M. Wang, S. Sun, T. Zhou, H. F. Ma, T. J. Cui, and Y. M. Liu, "Microwave-vortex-beam generation based on spoof-plasmon ring resonators," Phys. Rev. Appl. **13**, 054013 (2020).
[33]H. Feng, L. F. Ye, Y. Zhang, W. W. Li, H. Y. Chen, and Q. H. Liu, "Bidirectional multi-mode microwave vortex beam generation enabled by spoof surface plasmon polaritons," Appl. Phys. Lett. **117**, 241601 (2020).
[34]J. Petersen, J. Volz, and A. Rauschenbeutel, "Chiral nanophotonic waveguide interface based on spin-orbit interaction of light," Science **346**(6205), 67 (2014).
[35]P. Wang, Y. Wang, Z. Yang, X. Guo, X. Lin, X. C. Yu, Y. F. Xiao, W. Fang, L. Zhang, G. Lu, Q. Gong, and L. Tong, "Single-band 2-nm-line-width plasmon resonance in a strongly coupled Au nanorod," Nano Lett. **15**, 7581 (2015).
[36]S. I. Bozhevolnyi, V. S. Volkov, E. Devaux, J. Y. Laluet, and T. W. Ebbesen, "Channel plasmon subwavelength waveguide components including interferometers and ring resonators," Nature **440**, 508 (2006).
[37]J. E. Heebner and R. W. Boyd, "Enhanced all-optical switching by use of a nonlinear fiber ring resonator," Opt. Lett. **24**, 847 (1999).